Coal-ash Corrosion of Alloys for Combustion Power Plants*

K. Natesan
Argonne National Laboratory, 9700 South Cass Avenue, Argonne, IL 60439
E-mail: natesan@anl.gov; Telephone: (630) 252-5103; Fax: (630) 252-3604

A. Purohit and D. L Rink
Argonne National Laboratory, 9700 South Cass Avenue, Argonne, IL 60439
E-mail: purohit@anl.gov; Telephone: (630) 252-5949; Fax: (630) 252-3604

Abstract

A program on coal-ash corrosion is being conducted at Argonne National Laboratory to evaluate the performance of several structural alloys in the presence of mixtures of synthetic coal ash, alkali sulfates, and alkali chlorides. Candidate alloys are also exposed in a small-scale coal-fired combustor at the National Energy Technology Laboratory in Pittsburgh. Experiments in the present program, which addresses the effects of deposit chemistry, temperature, and alloy chemistry on the corrosion response of alloys, were conducted at temperatures in the range of 575-800°C for time periods up to ≈1850 h. Fe-base alloys selected for the study included HR3C, 310TaN, HR120, SAVE 25, NF709, modified 800, 347HFG, and HCM12A. In addition, 800H clad with Alloy 671 was included in several of the exposures. Ni-base alloys selected for the study included 600, 601, 617, 690, 625, 602CA, 214, 230, 45TM, HR 160, and 693. Data were obtained on weight change, scale thickness, internal penetration, microstructural characteristics of corrosion products, mechanical integrity of the scales, and cracking of scales. Results showed that the relationship of corrosion rates to temperature followed a bell-shaped curve for Fe-base alloys, with peak rates at ≈725°C, but the rate itself was dependent on the alloy chemistry. Several Fe-base alloys showed acceptable rates in the sulfate-containing coal-ash environment; but NaCl in the deposit led to catastrophic corrosion at 650 and 800°C. Ni-base alloys generally exhibited less corrosion than the Fe-base alloys under similar exposure conditions; however, they were susceptible to localized corrosion in the form of pits.

Background

Conceptual designs of advanced combustion systems that utilize coal as feedstock must include improved thermal efficiency and significant reduction in release of sulfur oxides, nitrogen oxides, and carbon dioxide. Such systems require materials and components that are capable of operating at much higher temperatures than those found in current coal-fired power plants. Component reliability and long-term, trouble-free performance of structural materials for these systems necessitate development/evaluation of materials in simulated coal-combustion environments. Apart from the environmental aspects of the effluent from coal combustion, one concern from the systems standpoint is the aggressiveness of the combustion environment toward boiler structural components such as steam superheaters and reheaters.

Recently, the U.S. Department of Energy has started to reevaluate coal-fired steam generation plants and, in particular, the designs based on supercritical and ultra-supercritical steam conditions. The ultimate goal of the staged development of power systems is to change steam pressure and temperature from the current values of 16.5-24 MPa (2400-3500 psig) and 540°C (1000°F), respectively, to 34.5 MPa (5000 psig) and 650°C (1200°F). Development of a revolutionary boiler design for U.S. markets, based on superheater/reheater temperatures >760°C, is also proposed. The higher steam temperature is expected to lead to another 2-3% increase in efficiency over a 700°C design, thus improving fuel usage and CO_2 emissions [1].

Fireside metal wastage in conventional coal-fired boilers can occur by gas-phase oxidation or deposit-induced liquid-phase corrosion. The former can be minimized by using materials that are resistant to oxidation at the service temperatures of interest. On the other hand, deposit-induced corrosion of materials is an accelerated type of attack, influenced by the

*Work supported by the U.S. Department of Energy, Office of Fossil Energy, Advanced Research Materials Program, Work Breakdown Structure Element ANL-4, under Contract W-31-109-Eng-38.

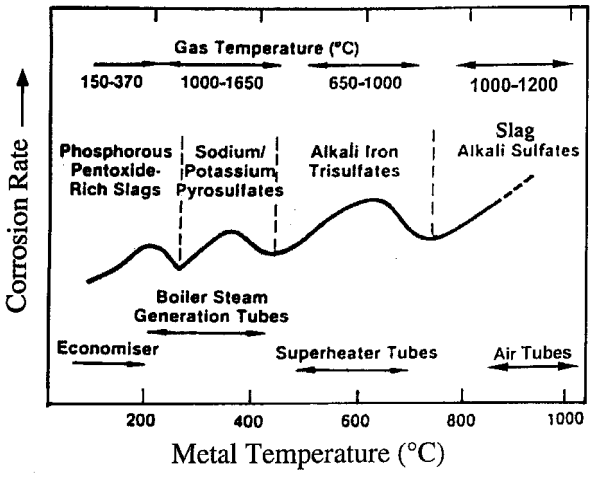

Figure 1. Regimes of fireside corrosion in coal-fired boilers.

vaporization and condensation of small amounts of impurities such as sodium, potassium, sulfur, chlorine, and vanadium (or their compounds) that are present in the coal feedstock. At the temperatures of interest in advanced combustion systems, mixtures of alkali sulfates, along with alkali chlorides, will dominate the fireside deposit, and viable structural alloys must be resistant to attack by such deposits. The temperature regimes in which this corrosion occurs are summarized in Figure 1.

Because most of the materials for application in boiler tubes are iron-based alloys, and because the mobility of iron from the alloy substrate to the scale/gas interface is fairly rapid, considerable attention has been given to understanding the formation of alkali-iron trisulfates and their role in the corrosion of steam superheaters in conventional boiler systems [2-4]. The effect of boiler deposits on the corrosion of structural materials has been fairly well established by Reid [2]. The sequence of events for alkali-iron-trisulfate-induced corrosion of iron-based materials begins with the formation of an oxide film on the metal surface, and/or oxidation of pyrite in the coal to form iron oxide and sulfur dioxide/sulfur trioxide gases. Alkali sulfates that originate from alkalis in the coal and sulfur oxides in the furnace atmosphere are deposited over the oxide scale on superheater materials. Eventually, because of an increasing temperature gradient, the outer surface of the alkali sulfate layer becomes sticky, and particles of fly ash are captured. With further increase in temperature, thermal dissociation of sulfur compounds in the ash releases SO_3 which migrates toward the cooler metal surface while a layer of slag forms on the outer surface. With more ash in the outer layer, the temperature of the sulfate layer falls, and reaction occurs between the oxide scale and SO_3, to form alkali-iron trisulfate. With this removal of the oxide scale, the metal oxidizes further. Deslagging due to temperature excursions or soot blowing to remove the deposits exposes the alkali-iron trisulfates to higher temperatures and leads to dissociation of sulfate and generation of SO_3 for further attack of the metal.

In advanced combustion systems, because the metals in the superheater regions will be subjected to much higher steam temperature, the alkali sulfate and coal ash will be the predominant deposit. Several factors (including sulfur, alkali, chlorine in coal feedstock; excess air level during the combustion process; and metal temperature) determine the extent of corrosion of superheater materials in coal-fired boilers. The objective of the present work is to evaluate the corrosion performance of state-of-the-art candidate materials in coal ash, alkali sulfate, and alkali chloride environments at temperatures in the range of 575-800°C. The experimental program is aimed at developing a scientific understanding of corrosion mechanisms as a function of alloy composition and deposit chemistry, and at quantitatively determining the scaling and internal penetration of the alloys.

Experimental Procedure

Numerous alloys, both ASME coded and uncoded, were selected for corrosion evaluation. The compositions of the Fe-base alloys selected for the study are listed in Table 1. Among those selected, HCM12A is a super ferritic alloy in which creep strength is obtained by both solution strengthening (W and Mo) and precipitation strengthening (V, Nb, and N). The alloy contains Cu (instead of Ni) to stabilize the long-term creep strength and to minimize δ-ferrite. The included austenitic alloys

were broadly based on 18-20Cr and 20-25Cr steels. Super 304H, 347HFG, and NF709 fall into 18-20Cr steels, with improved creep strength achieved by addition of Nb and/or Ti. HR3C, 310TaN, and SAVE 25 fall into 20-25Cr steels, with improved creep strength achieved by addition of Nb, Ti, Ta, and N. Modified 800 has the Alloy 800 base, with additions of the strengthening elements Nb, V, N, and B. HR120 is a Fe-Ni-Cr alloy with additions of Co, W, N, and Nb. In addition, specimens of 800H clad with Alloy 671 were also included in the study.

Table 2 lists the Ni-base alloys selected for the corrosion study. The alloys included 600, 601, 690, 617, 625, 602CA, 214, 230, 45TM, HR 160, and 693. Among them, Alloy 600 and 214 contained 15.4 and 15.9 wt.% Cr, respectively, whereas all the others contained Cr in a range of 21.5-28.8 wt.%. In addition, Alloys 617 and 625 had high concentration of Mo, Alloys 601, 602CA, and 214 contained Al concentration in a range of 1.4-3.7 wt.%; and Alloys 45TM and HR 160 contained Si in a range of 2.7-2.8 wt.%.

The specimens of various alloys, in the form of coupons ≈8-10 x 10 x 2 mm, were wet-ground with 600-grit SiC paper; they were identified by letters stamped at the corner of the coupons and were thoroughly degreased in clean acetone, rinsed in water, and dried.

A schematic diagram of the experimental setup used for the isothermal corrosion tests is shown in Figure 2. The experiments were conducted in a horizontal resistance-heated furnace that contained a 55-mm-i.d. x 3-mm-wall alumina reaction tube. The specimen was laid flat on a tray in the constant-temperature region of the chamber and was covered with a synthetic

Table 1. Nominal composition (in wt.%) of Fe-base alloys selected for corrosion study

Material	C	Cr	Ni	Mn	Si	Mo	Fe	Other
HCM12A	0.10	12	0.3	0.5	0.3	0.4	Bal	W 2.0, V 0.2, Nb 0.05, Cu 0.9, N 0.05
Super 304H	0.10	18	9	1.0	0.3	-	Bal	Nb 0.45, Cu 3.0, N 0.09
347HFG	0.08	18	11	2.0	1.0	-	Bal	Nb + Ta = 10 x C min
HR3C	0.06	25	20	1.2	0.4	-	Bal	Nb 0.45, N 0.2
310TaN	0.05	25	20	1.0	0.2	-	Bal	Ta 1.5, N 0.2
NF709	0.07	20	25	1.0	0.6	1.5	Bal	Ti 0.6, Nb 0.2, N 0.18, B 0.004
SAVE 25	0.10	23	18	1.0	0.4	-	Bal	Nb 0.45, W 1.5, Cu 3.0, N 0.2
Modified 800	0.10	20	30	1.5	0.2	1.5	Bal	Ti 0.25, Nb 0.25, V 0.05, N 0.03, B 0.004
HR120	0.05	25	37	0.7	0.6	2.5	Bal	Co 3, W 2.5, N 0.2, Cu, Al 0.1, Nb 0.7
MA956	-	20	-	-	-	-	Bal	Al 4.5, Ti 0.5, Y_2O_3 0.6
671-clad 800H								
671	0.05	48	Bal	0.02	0.2	-	0.2	Ti 0.4
800	0.05	21	32	0.5	0.2	-	Bal	Ti 0.4, Al 0.4

Table 2. Nominal composition (in wt.%) of Ni-base alloys selected for corrosion study

Material	C	Cr	Ni	Mn	Si	Mo	Fe	Other
600	0.04	15.4	Bal	0.2	0.1	-	9.7	-
601	0.03	21.9	Bal	0.2	0.2	0.1	14.5	Al 1.4, Ti 0.3, Nb 0.1
690	0.01	27.2	61.4	0.2	0.1	0.1	10.2	Ti 0.3, Al 0.2
617	0.08	21.6	53.6	0.1	0.1	9.5	0.9	Co 12.5, Al 1.2, Ti 0.3
IN 625	0.05	21.5	Bal	0.3	0.3	9.0	2.5	Nb 3.7, Al 0.2, Ti 0.2
602CA	0.19	25.1	62.6	0.1	0.1	-	9.3	Al 2.3, Ti 0.13, Zr 0.19, Y 0.09
214	0.04	15.9	Bal	0.2	0.1	0.5	2.5	Al 3.7, Zr 0.01, Y 0.006
230	0.11	21.7	60.4	0.5	0.4	1.4	1.2	W 14, Al 0.3, La 0.015
45TM	0.08	27.4	46.4	0.4	2.7	-	26.7	RE 0.07
HR 160	0.05	28.0	Bal	0.5	2.8	0.1	4.0	Co 30, Al 0.2
693	0.02	28.8	Bal	0.2	0.04	0.13	5.8	Al 3.3, Nb 0.67, Ti 0.4, Zr 0.03

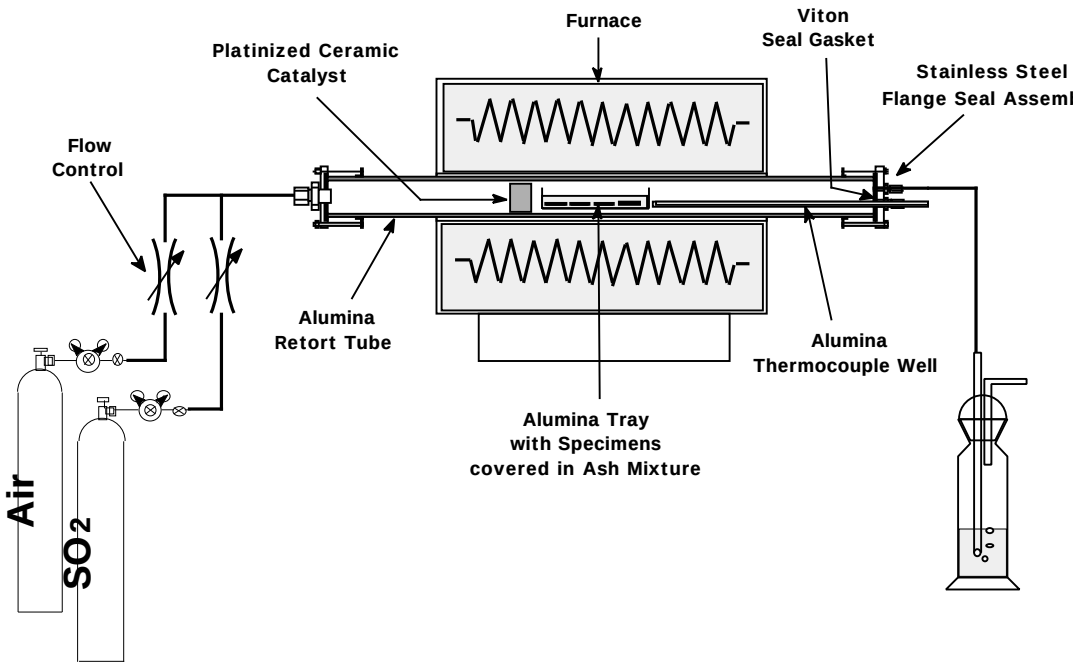

Figure 2. Schematic diagram showing furnace assembly, gas flow, and specimen arrangement used for corrosion experiments.

mixture of coal ash, alkali sulfates, and NaCl. The synthetic coal ash consisted of a mixture of reagent-grade SiO_2, Al_2O_3, and Fe_2O_3 in the ratio of 1:1:1 by weight. The alkali sulfate mixture consisted of Na_2SO_4 and K_2SO_4 in the ratio of 1:1 by weight. Three types of deposits were used in the corrosion experiments. In the first, ash and sulfate were mixed in the ratio of 90:10 by weight; in the second, ash, sulfate, and NaCl were mixed in the ratio of 85:10:5 by weight; in the third, ash, sulfate, and NaCl were mixed in the ratio of 89:10:1 by weight. The temperature was measured by a thermocouple inserted into an alumina thermowell that was fed through an opening in the flange of the reaction chamber. The specimens were exposed at temperatures of 575, 650, 725, and 800°C for time periods in the range of 336-1852 h. The experiments were generally stopped after either 168 or 336 h, and the specimens were cooled to room temperature, cleaned of the ash by brushing, and weighed. Specimen exposures were continued with a fresh supply of deposit mixture. Temperature was controlled to within ≈3°C in the vicinity of the specimens. A gas mixture of high-purity air that contained 1 vol.% SO_2 was fed through a Pt catalyst maintained at elevated temperature to ensure SO_2/SO_3 equilibrium in the gas mixture near the specimens.

Upon completion of the corrosion kinetics experiments, the specimens were examined by optical metallography and by a scanning electron microscope (SEM) equipped with energy–dispersive X–ray analyzer. In some cases, the deposit materials and the scales (developed on alloy specimens) were analyzed by X-ray diffraction. Optical examination of cross sections of exposed specimens and analyses with the SEM were used to identify the morphological features of corrosion-product phases in the scale layers and to establish the thickness of scales and depth of intergranular penetration, if any, in the alloys and cladding.

Results and Discussion

Corrosion Performance of Fe-base Alloys

At each exposure temperature, specimens of various alloys were exposed to a mixture of coal ash and alkali sulfate for 168 or 336 h, after which the specimens were retrieved, cleaned of deposit, and weighed. Subsequently, the exposures were continued with a fresh deposit mixture for another 168 or 336 h. The procedure was repeated several times at various

temperatures to accumulate weight change data, which was plotted as a function of exposure time to develop a corrosion rate at each temperature for each alloy. In general, the weight change followed linear kinetics for all the Fe-base alloys. At temperatures of 575, 650, and 725°C, most of the alloys lost weight, and the losses were strongly dependent on the alloy composition. At 800°C, several of the Fe-base alloys gained weight, and a few of them lost weight, but not to the same extent as observed at 725°C.

Weight change data for several Fe-base alloys tested at temperatures between 575 and 800°C in deposits containing 0 and 5 wt.% NaCl were presented in an earlier report [5]. The results indicated that the weight loss rates increased with temperature up to 725°C and decreased to low values at 800°C. In fact, several of the alloys showed either negligible weight loss and/or gained weight after exposure at 800°C. The corrosion rates followed a bell-shaped curve with peaks near 725°C for all of the Fe-base alloys studied. Weight loss rates for several alloys at 650 and 800°C, obtained when exposed in a deposit mixture that contained 5 wt.% NaCl, were also reported earlier [5]. The weight loss data indicated that the presence of 5 wt.% NaCl in the deposit had little effect on the corrosion rate at 650°C, and that most of the alloys exhibited similar weight loss rates after exposure in deposits with and without NaCl. On the other hand, at 800°C, several alloys exhibited accelerated corrosion in the presence of deposit that contained NaCl, when compared with the same alloys in the absence of NaCl.

Total corrosion (scale thickness plus penetration) data were reported earlier for several Fe-base alloys after exposure at 650, 725, and 800°C in an environment that contained coal ash and alkali sulfate [5]. Results showed that at 650°C alloys such as 347HFG, SAVE25, and 800H exhibited total corrosion rate <0.2 mm/y, and all of the other alloys showed rates ≤0.44 mm/y. At 725°C, the corrosion rate for all of the alloys increased, and several of them exhibited a dramatic increase. For example, the rates for SAVE25 and modified 800H were 2.1 and 1.65 mm/y, respectively. At 800°C, the corrosion rates for several alloys slightly decreased from the values obtained at 725°C. Results indicated that NF709 was a superior-performing alloy, with rates of 0.26, 0.25, and 0.55 mm/y at 650, 725, and 800°C, respectively. The corresponding values for 310 TaN were 0.43, 0.50, and 0.55 mm/y, respectively. The effect of 5 wt.% NaCl in the deposit mixture on the corrosion performance showed that NaCl accelerated corrosion in all of the Fe-base alloys used in this study. NF709, the best-performing alloy in the absence of NaCl, had corrosion rates of 2 and 15 mm/y at 650 and 800°C in the presence of NaCl. The best-performing alloy in environments with and without NaCl was HR3C. The corrosion rates of this alloy were 0.37 and 0.7 mm/y at 650°C in environments without and with 5 wt.% NaCl, respectively.

The causes for accelerated corrosion in the heat resistant alloys in the presence of NaCl are two fold. The NaCl in the deposit mixture establishes within the deposit mixture a Cl activity, which can attack the carbides that are present in the alloy as strengtheners. Furthermore, the Cl activity in the deposit near the alloy can be high enough to form volatile chlorides of Fe, Cr, and Al (if present in the alloy). The volatile chlorides lead to a porous microstructure with virtually no scale development to protect the alloy.

To examine the influence of NaCl concentration in the deposit on the corrosion performance of Fe-base alloys, additional tests were conducted at 650, 725, and 800°C with a deposit that contained 1 wt.% NaCl. One major difference between the experiments conducted in the presence of Ash 1 (with no NaCl) and Ash 3 (with 1 wt.% NaCl) is the stickiness and adherence of the deposit with the substrate alloy. The deposit was significantly more adherent in the presence of NaCl than the absence of NaCl. This was evident in the measured weight change data developed as a function of exposure time. Figure 3 shows the weight change data as a function of exposure time for several alloys tested at 725 and 650°C in the presence of Ash 1. The data indicate a monotonically decreasing weight of the specimens, which is essentially linear with time. Figure 4 shows the weight change data as a function of exposure time for alloys HR3C and NF709 tested at 650°C in the presence of Ash 3. Figure 5 shows the weight loss rates for nine alloys at temperatures between 650 and 800°C, obtained when exposed in a deposit mixture that contained 1 wt.% NaCl. A comparison of the data for a deposit containing 1 wt.% NaCl with earlier-reported data for a deposit containing 5 wt.% NaCl showed that the alloy weight losses are much less with the lower concentration of NaCl. The weight change data may not be representative of the corrosion process in the latter specimens, primarily because of the stickiness of the deposit and the inability to clean the deposit off the specimens without damaging the corrosion product layers.

The data in Figures 3-5 should only be used qualitatively, because the weight loss rates can be affected by the removal of scales during removal of coal ash deposit from the specimen surface, even though every effort was made to remove only the ash deposits by brushing. Generally, the scales adhered more to some alloys than others and adhered more in the presence than the absence of NaCl, and caution should be exercised in using this information for corrosion allowance for components.

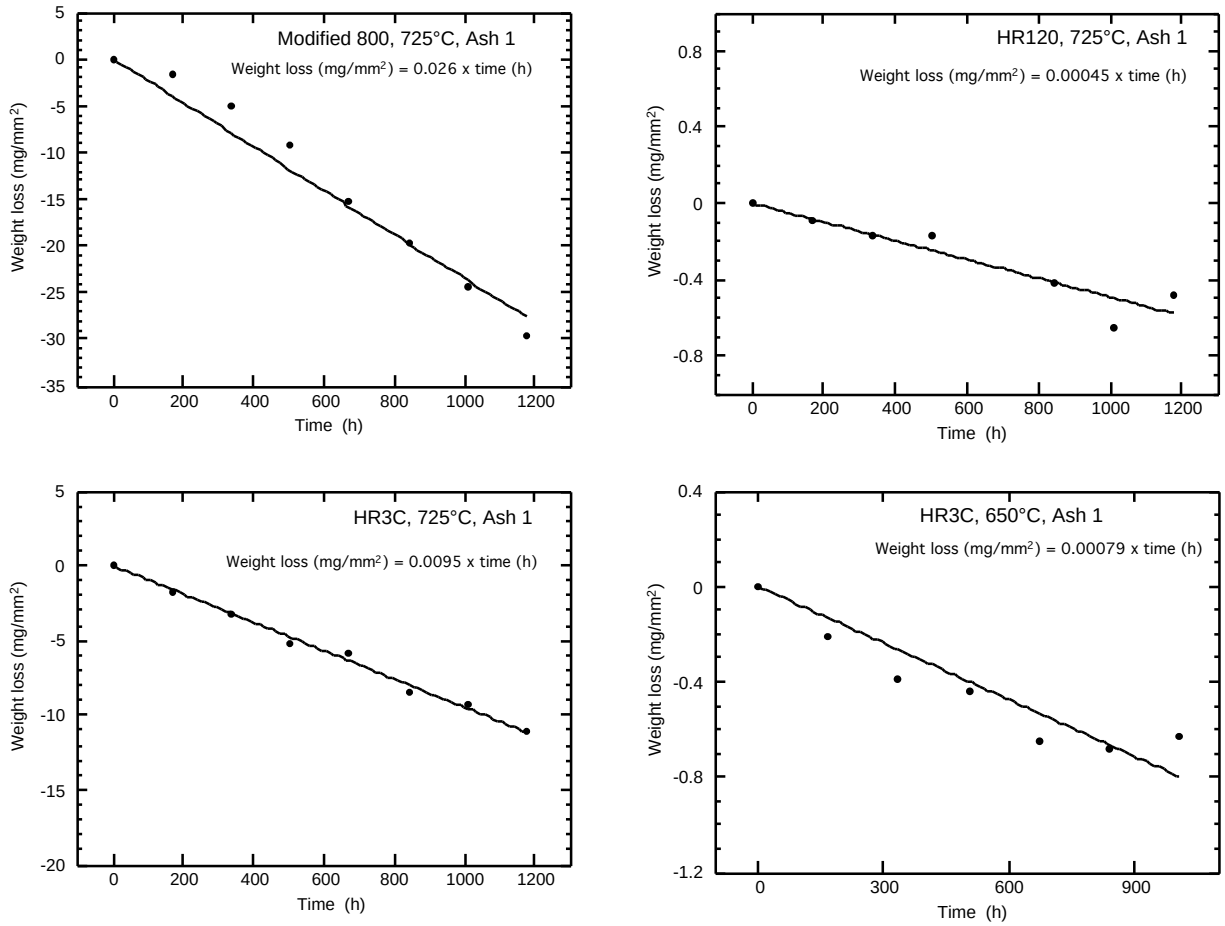

Figure 3. Weight change data obtained as a function of exposure time for modified 800H, HR 120, and HR3C at 725°C and for HR3C at 650°C, in the presence of Ash 1.

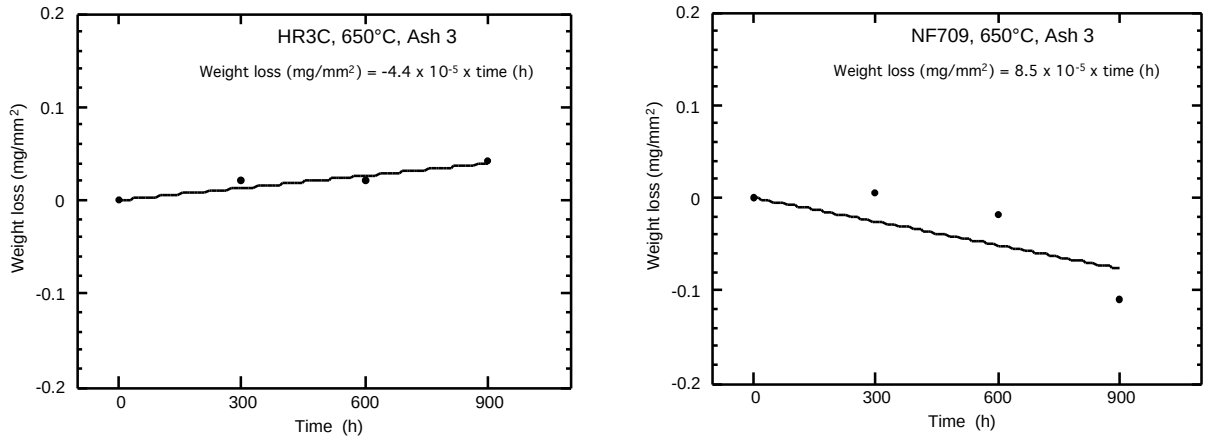

Figure 4. Weight change data obtained as a function of exposure time for HR3C and NF709 at 650°C, in the presence of Ash 3.

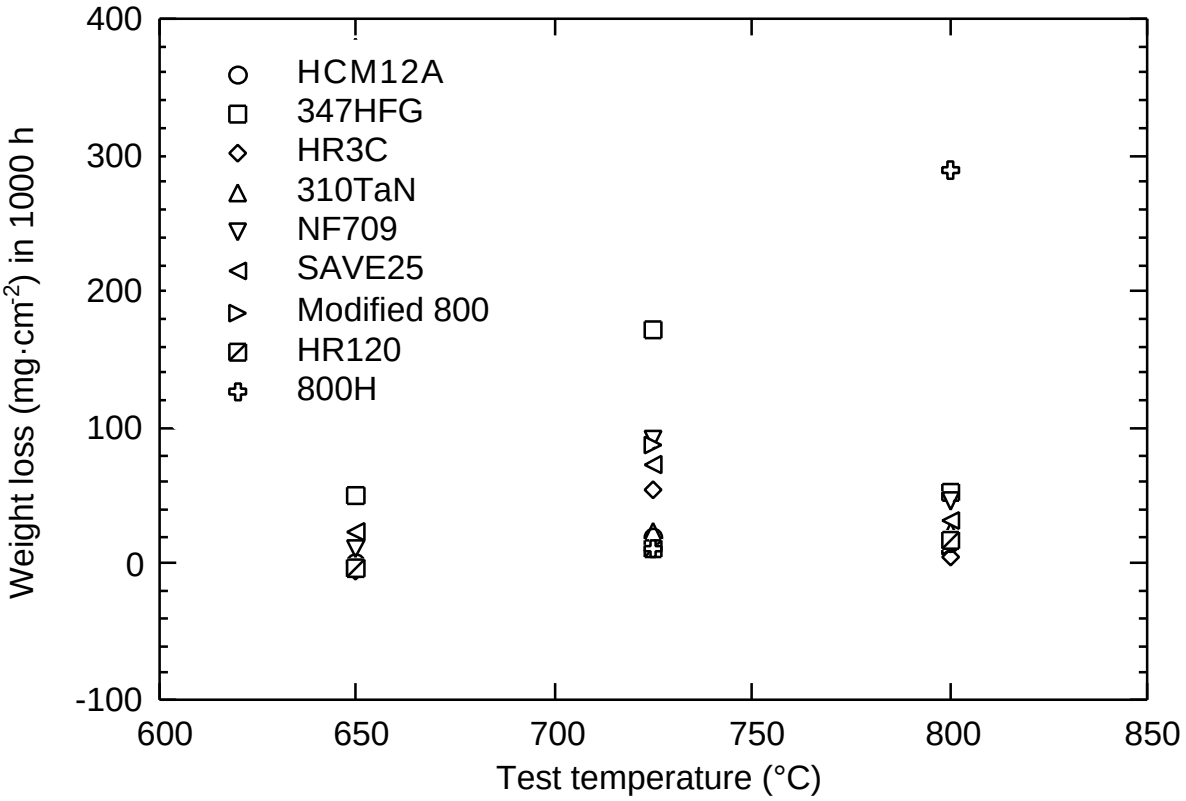

Figure 5. Weight loss data for Fe-base alloys after exposure in a mixture of synthetic coal ash, alkali sulfates, and 1 wt.% NaCl at temperatures between 650 and 800°C.

Therefore, all of the tested alloys were mounted and polished to examine the rates of scaling and internal penetration in the alloys using optical and scanning electron microscopy. Figure 6 shows the total corrosion (scale thickness plus penetration) for Fe-base alloys after exposure at 650 in the presence of deposits that contained 0 (Ash 1), 1 (Ash 3), and 5 (Ash 2) wt.% NaCl.

Microstructural Observations

Extensive analysis was presented earlier on the microstructural aspects of scaling and internal penetration in Fe-base alloys [5]. We also presented SEM photomicrograph (see Fig. 7) of the cross section of Inconel 671-clad Alloy 800 specimen that was exposed to Ash 1 (a mixture of ash constituents and alkali sulfate) showing significant attack on the Alloy 800 side of the specimen. Figure 8 shows the SEM photomicrograph of the cross section of a similar specimen after 900-h exposure at 650°C in Ash 3, which contained 1 wt.% NaCl. The susceptibility of Alloy 800 to corrosion is evident from these figures. Figure 9 shows an SEM micrograph of the cross section of Alloy MA956 that was tested in Ash 3, showing significant pitting attack and internal penetration.

Corrosion Performance of Ni-base Alloys

Exposures of Ni-base alloys followed a procedure similar to that used for the Fe-base alloys. The Ni-base alloys were tested in two deposit mixtures identified as Ash 1 (a mixture of ash constituents and 10 wt.% alkali sulfate) and Ash 3 (Ash 1 plus 1 wt.% NaCl). Figures 10 and 11 show the weight change measured for various Ni-base alloys that were exposed for 1680 h to deposits containing ash constituents, alkali sulfates, and 0 and 1 wt.% NaCl, respectively. The results indicate that the weight loss rates are significantly lower than those observed for the Fe-base alloys under similar exposure conditions. However, the

results are misleading for two reasons. The deposits (due to their stickiness) are much more adherent to the scale and substrate in the case of Ni-base alloys than the Fe-base alloys, and effective removal of the deposit is difficult. Furthermore, the corrosive attack in the case of Ni-base alloys is more localized in the form of pits, which can be rather large and deep and may not be reflected in the overall weight change of the specimen.

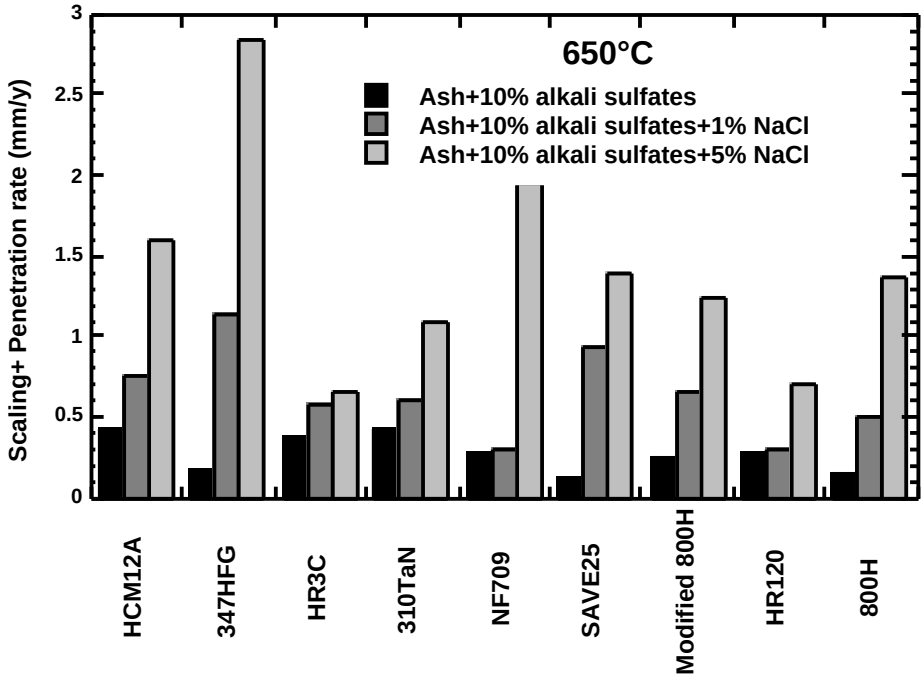

Figure 6. Scaling rate plus penetration rate for several Fe-base alloys after exposure at 650°C in presence of deposits containing 0, 1, and 5 wt.% NaCl.

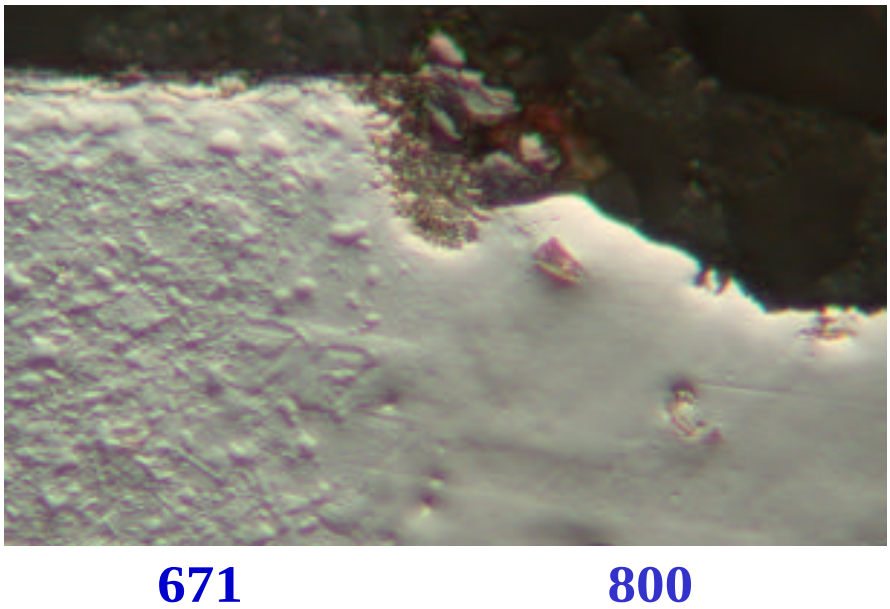

Figure 7. Scanning electron photomicrograph of Inconel 671-clad Alloy 800 specimen after 668-h exposure at 650°C to a mixture of ash and alkali sulfates (Ash 1).

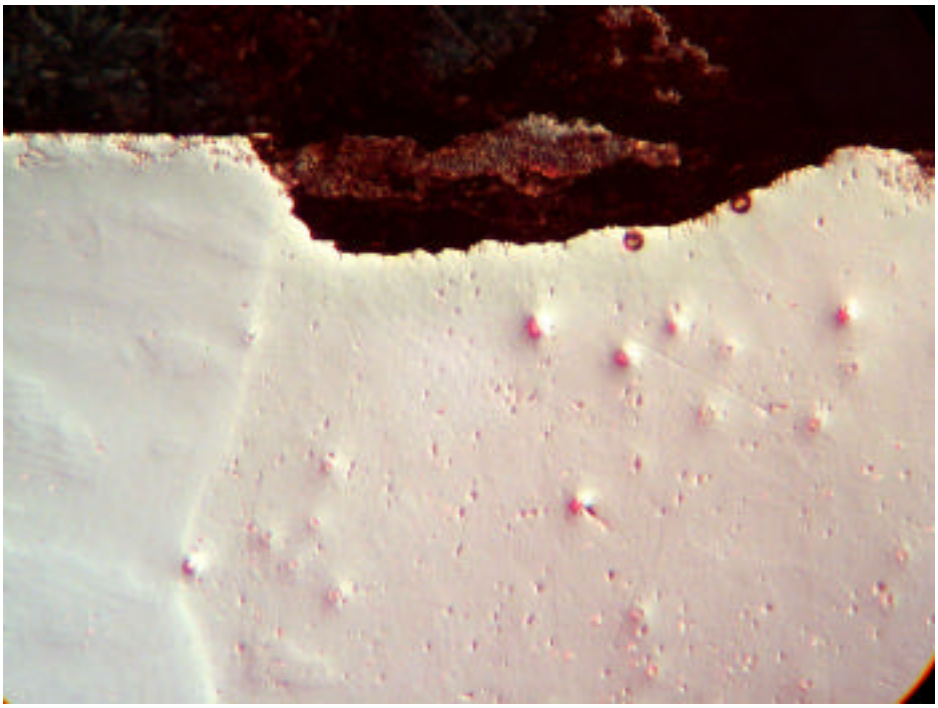

Figure 8. Scanning electron photomicrograph of Inconel 671-clad Alloy 800 specimen after 900-h exposure at 650°C to a mixture of ash, alkali sulfates, and 1 wt.% NaCl (Ash 3).

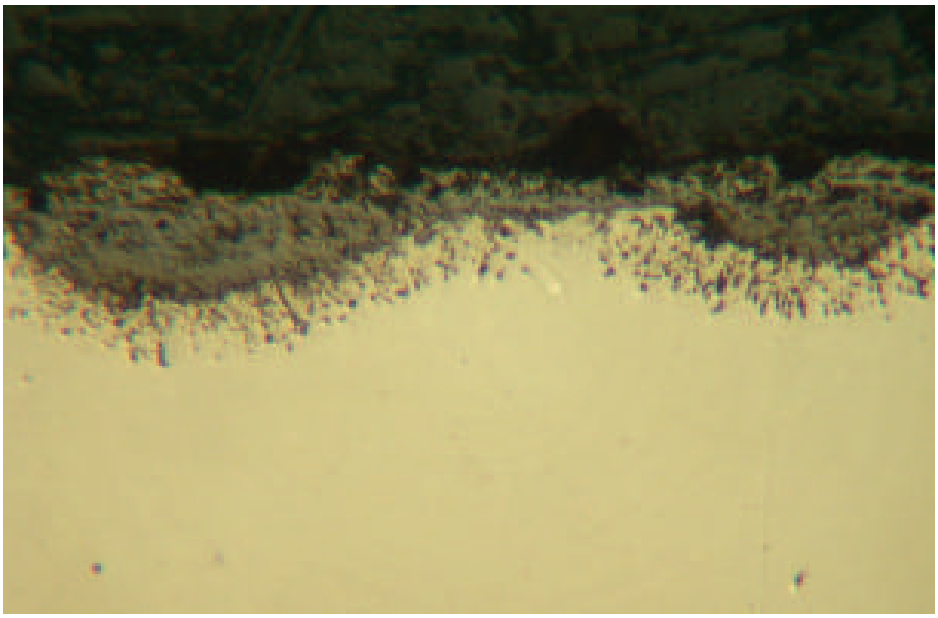

Figure 9. Scanning electron photomicrograph of MA 956 specimen after 900-h exposure at 650°C to a mixture of ash, alkali sulfates, and 1 wt.% NaCl (Ash 3).

Figure 12 shows the total corrosion (scale thickness plus penetration) for Ni-base alloys after exposure at 650°C in the presence of deposits that contained 0 (Ash 1) and 1 (Ash 3) wt.% NaCl. Results show that several of the alloys exhibit total corrosion rates <0.3 mm/y, based on parabolic kinetics. The measured corrosion rates include penetration depth values that were observed in the pits and represent maximum rates for these alloys. A comparison of the data in Figure 12 with those for

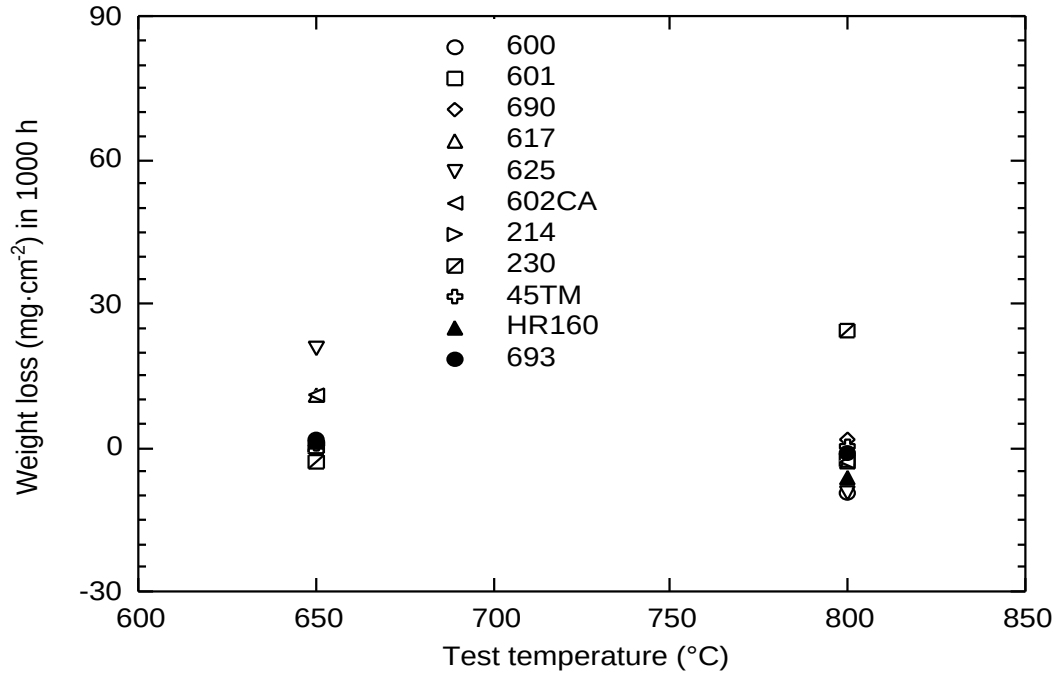

Figure 10. Weight loss data for Ni-base alloys after exposure in a mixture of synthetic coal ash and alkali sulfates at 650 and 800°C.

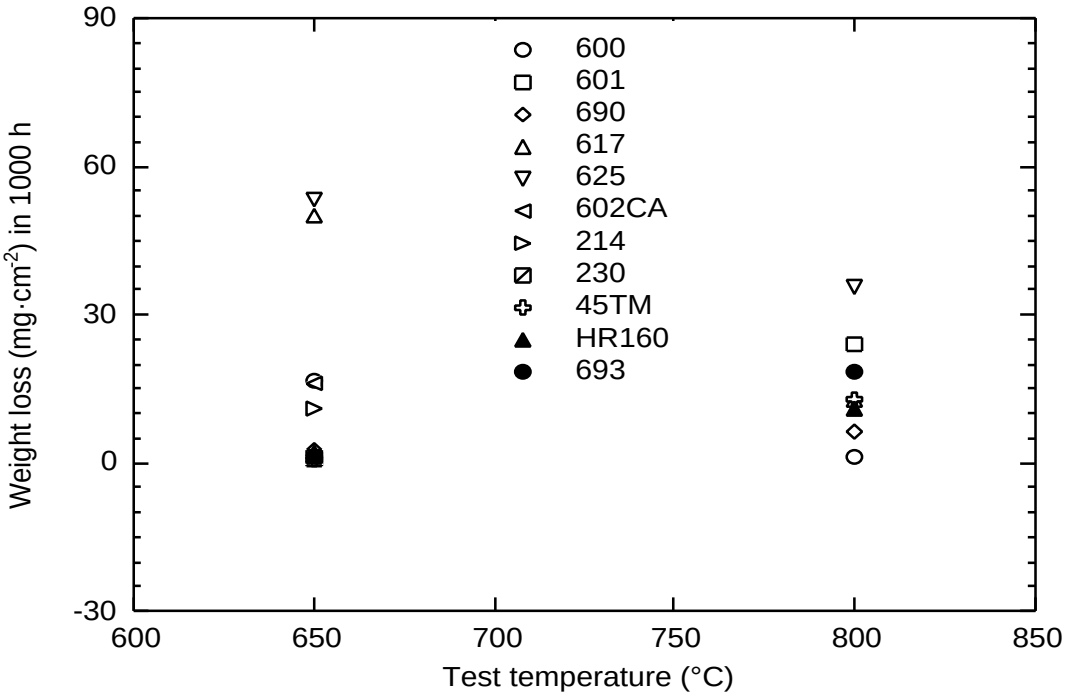

Figure 11. Weight loss data for Ni-base alloys after exposure in a mixture of synthetic coal ash, alkali sulfates, and 1 wt.% NaCl at 650 and 800°C.

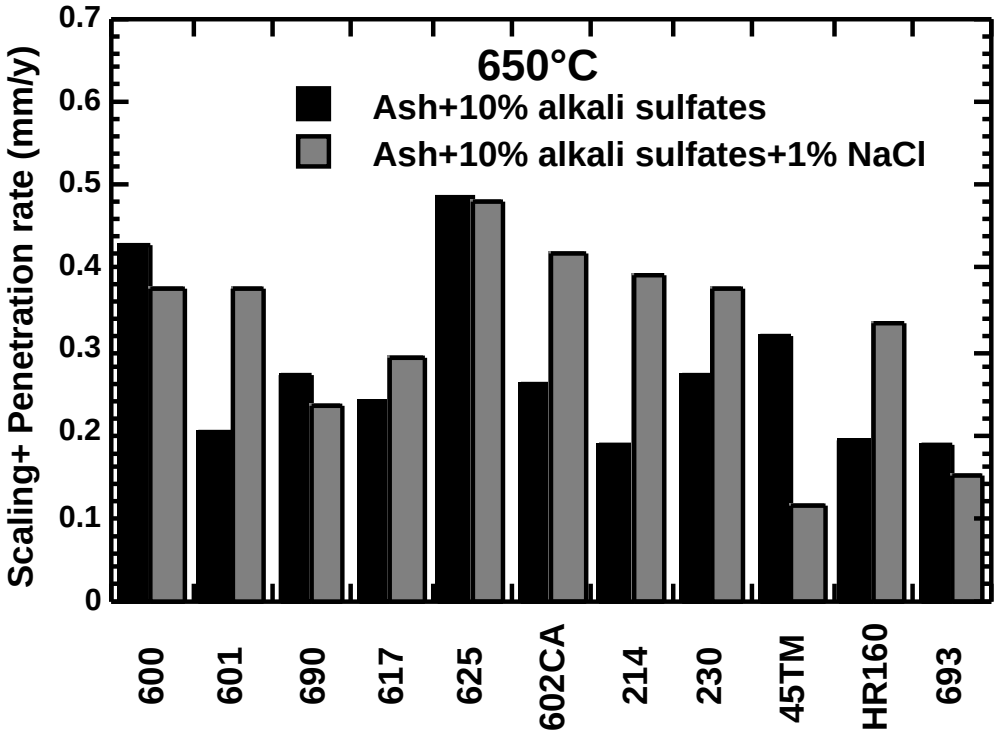

Figure 12. Scaling rate plus penetration rate for Ni-base alloys after exposure at 650°C in the presence of deposits containing ash constituents and alkali sulfates, with and without 1 wt.% NaCl.

Fe-base alloys (Fig. 6) indicates that the rates for the Ni-base alloys are generally much lower at 650°C, even in the presence of 1 wt.% NaCl. Nickel-base alloys are expected to resist chloride attack because the vapor pressure of $NiCl_2$ is much lower than that of Fe, Cr, and Al chlorides for the same Cl activity and gas temperature [6, 7]. Additional work is planned at higher temperatures to evaluate corrosion performance of Ni-base alloys in the presence of deposits with and without NaCl.

Microstructural Observations

Extensive analysis was performed on the microstructural aspects of scaling and internal penetration in Ni-base alloys tested at 650°C in the presence of deposits with and without NaCl addition. Figures 13 and 14 show SEM photomicrographs of cross sections of 625, 602CA, 230, and 45TM specimens after 1680-h exposure to a deposit containing ash constituents and alkali sulfates (Ash 1). The pits seen in these photomicrographs are representative of the size and depth observed in these specimens, and multitude pits appeared on all of the specimens after the 1680-h exposure. Figures 15 and 16 show SEM photomicrographs of cross sections of 230 and 45TM specimens after the 1680-h exposure to a deposit containing ash constituents, alkali sulfates, and 1 wt.% NaCl (Ash 3). The results indicate that the presence of 1 wt.% NaCl in the deposit had little affect either on the morphology of the corroded region or on the depth of pitting and intergranular attack for the Ni-base alloys. This finding is contrary to the severe increase in attack observed in the presence of 1 wt.% NaCl for the Fe-base alloys.

Figures 16 and 17 show the SEM photomicrographs of Alloy 601 specimen after 1680-h exposure in the presence of Ash 1 and Ash 3, respectively, along with X-ray mapping for several elements in the corroded regions. It is evident that the oxide scales are not protective in both environments, and the pitted regions exhibit significant sulfidation attack. The mechanism for corrosion of Ni-base alloys in the presence of alkali sulfates and alkali chlorides is well established in the corrosion

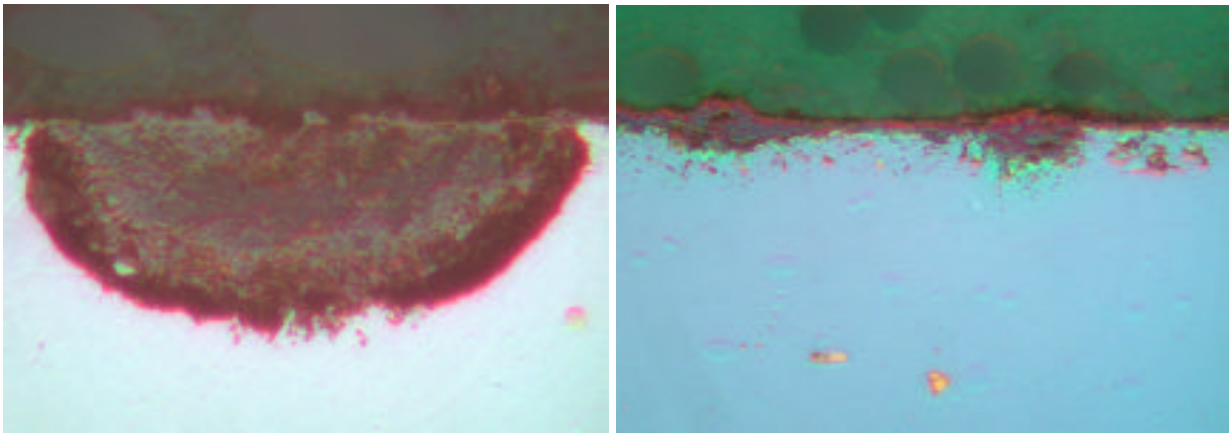

Figure 13. Scanning electron photomicrograph of 625 (left) and 602CA (right) specimens after 1680-h exposure at 650°C to a mixture of ash and alkali sulfates (Ash 1).

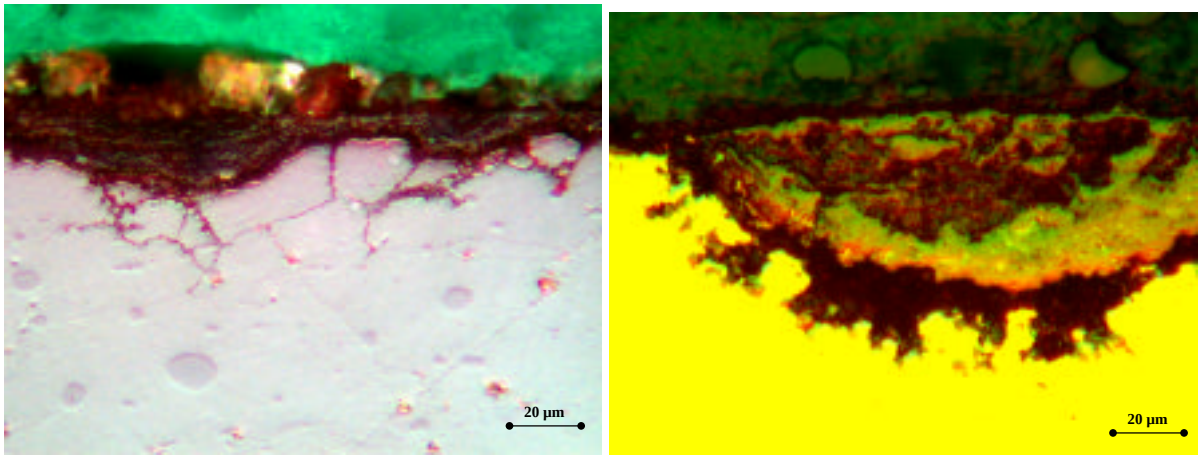

Figure 14. Scanning electron photomicrograph of 230 (left) and 45TM (right) specimens after 1680-h exposure at 650°C to a mixture of ash and alkali sulfates (Ash 1).

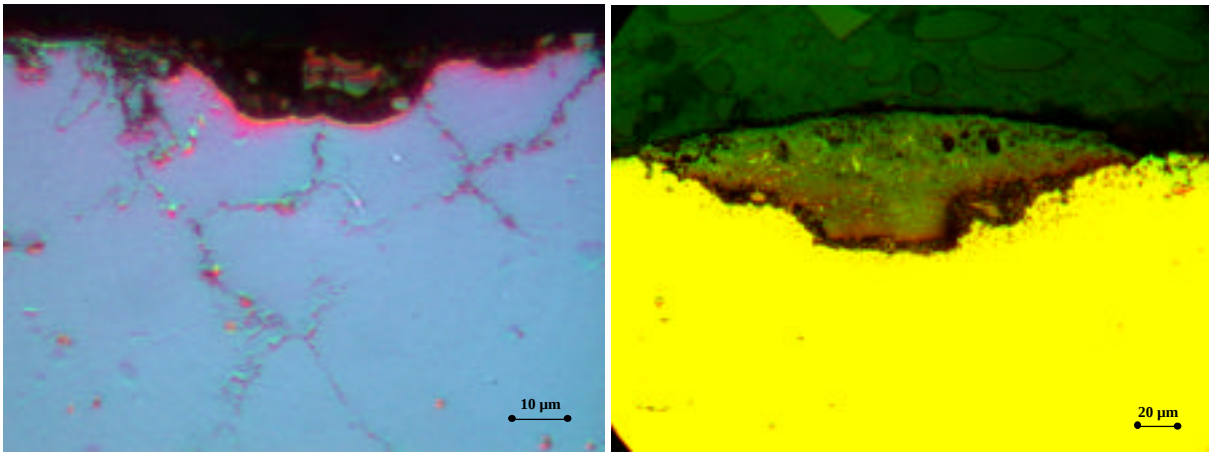

Figure 15. Scanning electron photomicrograph of 230 (left) and 45TM (right) specimens after 1680-h exposure at 650°C to a mixture of ash, alkali sulfates, and 1 wt.% NaCl (Ash 3).

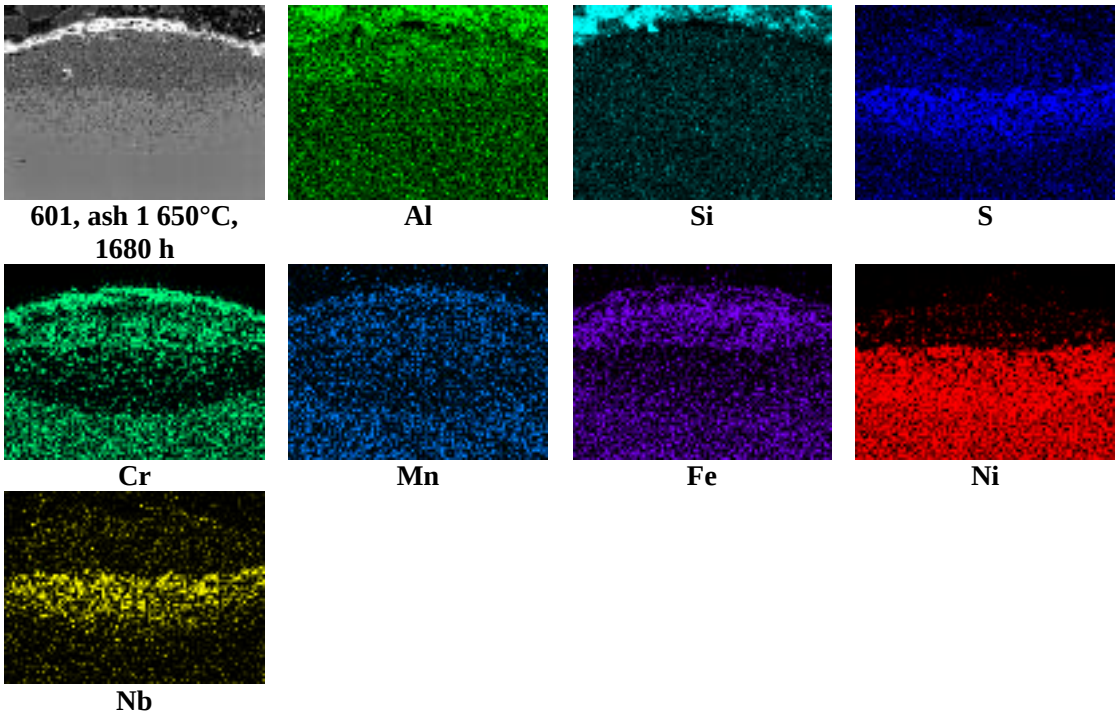

Figure 16. Scanning electron photomicrograph of 601 and elemental mapping for Al, Si, S, Cr, Mn, Fe, Ni, and Nb after 1680-h exposure at 650°C to a mixture of ash and alkali sulfates (Ash 1).

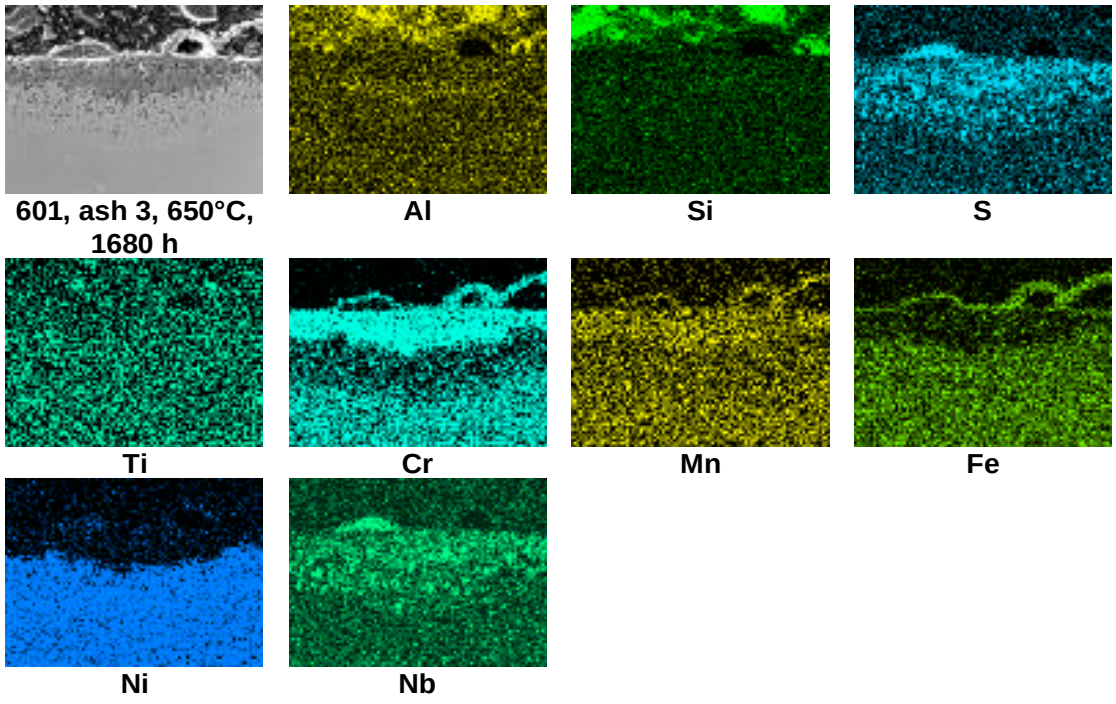

Figure 17. Scanning electron photomicrograph of 601 and elemental mapping for Al, Si, S, Ti, Cr, Mn, Fe, Ni, and Nb after 1680-h exposure at 650°C to a mixture of ash, alkali sulfates, and 1 wt.% NaCl (Ash 3).

studies conducted for gas turbine applications. The mechanism is termed "low-temperature hot corrosion," which occurs by formation of liquid phases involving alkali sulfates and base-metal sulfates, which accelerate the corrosion process. Figure 18 shows the X-ray diffraction (XRD) patterns for the corrosion product retrieved from the surface of Alloy 617 after 1680-h exposure at 650°C in the presence of Ash 1 and Ash 3 deposits. The diffraction patterns clearly indicate presence of $NiSO_4$ phase in the layer, supporting degradation by "low-temperature hot corrosion".

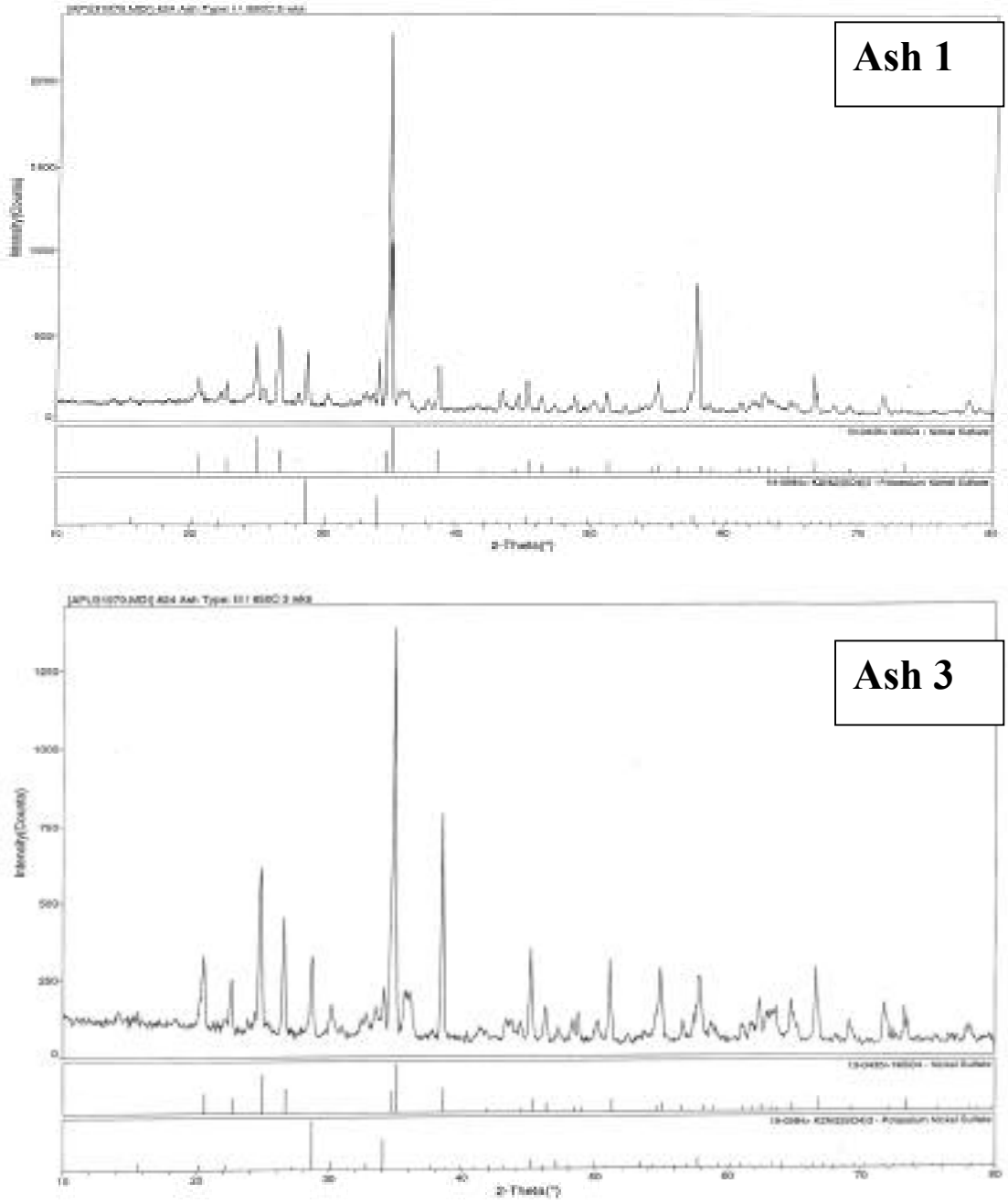

Figure 18. X-ray diffraction data of corrosion-product layers for Alloy 617 after 1680-h exposure at 650°C to a mixture of ash, alkali sulfates, and 0 (Ash 1) and 1 wt.% NaCl (Ash 3).

Summary

Fireside corrosion is a major issue when selecting materials for advanced steam-cycle systems. We have conducted studies at Argonne National Laboratory to evaluate the corrosion performance of candidate Fe-base and Ni-base alloys in coal-ash environments. The laboratory tests simulated the combustion atmosphere of advanced steam-cycle systems and three deposit chemistries, which included ash constituents, alkali sulfates, and NaCl. Corrosion rate data showed a bell-shaped curve for the Fe-base alloys, with peak rates at ≈725°C, and the rate itself was dependent on the alloy chemistry. Several alloys showed acceptable rates in the sulfate-containing coal-ash environment; but NaCl in the deposit led to catastrophic corrosion at 650 and 800°C. To attain acceptable corrosion, it is essential to establish maximum levels for alkali sulfates and alkali chlorides in combustion environments (and their relationship to coal feedstock). The data obtained on Ni-base alloys at 650°C showed the corrosion rates for these alloys to be significantly less than those of Fe-base alloys for the same exposure conditions. However, the type of attack in the Ni-base alloys was much more localized in the form of pits. Detailed microstructural examination and XRD analysis of the corrosion product layers indicate that Ni-base alloys corroded via a "low-temperature hot corrosion" mechanism that involves formation of liquid alkali sulfate and base metal sulfate eutectic. This reaction leads to sulfidation attack of the structural alloy. Additional tests are in progress to evaluate the corrosion performance of Ni-base alloys at higher temperatures. Attaining adequate creep strength, fireside corrosion resistance, and steam-side corrosion resistance is still a challenge in materials development for advanced steam-cycle applications.

References

[1]. R. Viswanathan and W. Bakker, J. Mater. Eng. Perf. 10 (1), 2001, 81.
[2]. W. T. Reid, External Corrosion and Deposits, American Elsevier, New York, 1971.
[3]. E. A. Sondreal, G. H. Gronhovd, P. H. Tufte, and W. Beckering, Ash Deposits and Corrosion Due to Impurities in Combustion Gases, R. W. Bryers, ed., Hemisphere Publishing Corp., Washington, D.C., p. 85, 1978.
[4]. R. W. Borio and A. L. Plumley, W. R. Sylvester, ibid, p. 163.
[5]. K. Natesan, A. Purohit, and D. L. Rink, Fireside Corrosion of Alloys for Combustion Power Plants, Proc. 16th Annual Conference on Fossil Energy Materials, Baltimore, MD, April 22-24, 2002.
[6]. K. Natesan and C. Reignier, Corrosion Performance of Structural Alloys in Oxygen/Sulfur/Chlorine-Containing Environments, Proc. 12th Ann. Conf. on Fossil Energy Materials, Knoxville, Paper 1.8, 1998.
[7]. K. Natesan and C. Kraus, Corrosion Performance of Structural Alloys and Coatings in the Presence of Deposits, Proc. 15th Ann. Conf. on Fossil Energy Materials, Knoxville, 2000.

Acknowledgments

This work was supported by the U.S. Department of Energy, Office of Fossil Energy, Advanced Research Materials Program, Work Breakdown Structure Element ANL–4, under Contract W–31–109–Eng–38. Paul Johnson of the ANL Analytical Chemistry Laboratory performed the XRD analysis of the deposits and corrosion-product layers.